International Journal of Pharmaceutics 644 (2023) 123315

Contents lists available at ScienceDirect

International Journal of Pharmaceutics

journal homepage: www.elsevier.com/locate/ijpharm

Praziquantel meets Niclosamide: A dual-drug Antiparasitic Cocrystal

Ilenia D'Abbrunzo [a], Emma Bianco [a], Lara Gigli [b], Nicola Demitri [b], Rebecca Birolo [c], Michele R. Chierotti [c], Irena Škorić [d], Jennifer Keiser [e,f], Cécile Häberli [e,f], Dario Voinovich [a], Dritan Hasa [a,*], Beatrice Perissutti [a,*]

[a] Department of Chemical and Pharmaceutical Sciences, University of Trieste, P.le Europa 1, 34127 Trieste, Italy
[b] Elettra-Sincrotrone Trieste, S.S. 14 Km 163.5 in Area Science Park, Basovizza–Trieste, Italy
[c] Department of Chemistry and NIS Centre, University of Torino, V. Giuria 7, 10125 Torino, Italy
[d] Department of Organic Chemistry, Faculty of Chemical Engineering and Technology, University of Zagreb, Marulićev trg 19, 10000 Zagreb, Croatia
[e] Department of Medical Parasitology, Swiss Tropical and Public Health Institute, 4123 Allschwil, Switzerland
[f] University of Basel, Basel 4000, Switzerland

ARTICLE INFO

Keywords:
Dual-drug cocrystal
Praziquantel-Niclosamide cocrystal
Cocrystal structure solution
In vitro anthelmintic activity
In vivo preliminary tests
Minicapsules size M

ABSTRACT

In this paper we report a successful example of combining drugs through cocrystallization. Specifically, the novel solid is formed by two anthelminthic drugs, namely praziquantel (PZQ) and niclosamide (NCM) in a 1:3 molar ratio, and it can be obtained through a sustainable one-step mechanochemical process in the presence of micromolar amounts of methanol. The novel solid phase crystallizes in the monoclinic space group of $P2_1/c$, showing one PZQ and three NCM molecules linked through homo- and heteromolecular hydrogen bonds in the asymmetric unit, as also attested by SSNMR and FT-IR results. A plate-like habitus is evident from scanning electron microscopy analysis with a melting point of 202.89 °C, which is intermediate to those of the parent compounds. The supramolecular interactions confer favorable properties to the cocrystal, preventing NCM transformation into the insoluble monohydrate both in the solid state and in aqueous solution. Remarkably, the PZQ - NCM cocrystal exhibits higher anthelmintic activity against in vitro S. *mansoni* models than corresponding physical mixture of the APIs. Finally, due to in vitro promising results, in vivo preliminary tests on mice were also performed through the administration of minicapsules size M.

1. Introduction

Cocrystallization of two active pharmaceutical ingredients (APIs) (drug-drug cocrystals) has recently emerged as an innovative drug development strategy, representing a new approach to develop multi-drug solid forms (Port et al., 2019; Thakuria and Sarma, 2018; Thipparaboina et al., 2016). It has been already observed that such innovative systems are more advantageous compared to the traditional multimodal therapy, i.e., fixed-dose combinations (FDCs) that are nothing but physical mixtures of the constituent APIs, presenting important stability issues and differences of solubilization kinetics among the combined drugs (Sarmah et al., 2020; Song et al., 2020; Thakuria et al., 2013; Žegarac et al., 2014).

Contrary to FDCs, drug-drug cocrystals are unique stable crystalline solid phases with a similar dissolution profile that can (positively) affect the pharmacokinetic and pharmacodynamic parameters (Port et al., 2019; Thipparaboina et al., 2016).

Importantly, drug-drug cocrystals may allow coadministration of two active ingredients thus providing pill load reduction and decreasing the risk of side effects or drug resistance phenomena (Deka et al., 2021). Another direct advantage consists of a simplification of the drug dosage thus improving patient compliance that is often low in traditional

Abbreviations: APIs, active pharmaceutical ingredients; PZQ, praziquantel; NCM, niclosamide; FCDs, fixed-dose combination; BCS, Biopharmaceutics Classification System; DSC, differential scanning calorimetry; XRPD, X-ray powder diffraction; FT-IR, infrared spectroscopy; SSNMR, solid-state NMR; SXRD, single-crystal X-ray diffraction; SEM, scanning electron microscopy; NTS, Newly Transformed Schistosomula; *S. mansoni*, adult *Schistosoma mansoni*; WBR, worm burden reduction; MeOH, methanol; EA, ethyl acetate; HXN, hexane; EtOH, ethanol; IsOH, isopropanol; TEG, triethylene glycol; AcT, acetone; ACN, acetonitrile; 2-pyr, 2-pyrrolidone; DMSO, dimethyl sulfoxide; TMS, tetramethyl silane; ASU, asymmetric unit.

* Corresponding authors at: Department of Chemical and Pharmaceutical Sciences, University of Trieste, P.le Europa 1, 34127 Trieste, Italy.
E-mail addresses: s244105@ds.units.it (I. D'Abbrunzo), lara.gigli@elettra.eu (L. Gigli), nicola.demitri@elettra.eu (N. Demitri), michele.chierotti@unito.it (M.R. Chierotti), dhasa@units.it (D. Hasa), bperissutti@units.it (B. Perissutti).

https://doi.org/10.1016/j.ijpharm.2023.123315
Received 18 May 2023; Received in revised form 6 July 2023; Accepted 11 August 2023
Available online 12 August 2023

combination drugs (Wang et al., 2021). Finally, these multicomponent systems may lead to a simplification in terms of formulation by improving stability and tabletability (Port et al., 2019).

In this context, we report the cocrystallization of Praziquantel (PZQ) (Fig. 1a) and Niclosamide (NCM) (Fig. 1b) to obtain an API-API antiparasitic cocrystal. PZQ is an anthelminthic drug largely used for the treatment of Schistosomiasis, that is an infection caused by trematodes of the genus Schistosoma (Cioli et al., 2014), while NCM is mainly applied to cure parasite infestations, such as those of tapeworms and cestode (Luedeker et al., 2016).

Both PZQ and NCM belong to class II of the Biopharmaceutics Classification System (BCS) thus showing low solubility and high permeability (Lindenberg et al., 2004). Therefore, the synthesis of a PZQ-NCM cocrystal may represent a promising route to improve APIs solubility and create a simplified antiparasitic therapy.

PZQ-NCM cocrystal was initially obtained through mechanochemistry, and the optimization of the process was achieved through the variation of one process variable at a time. Subsequently, a single crystal was obtained through solution crystallization of the mechanochemical product. The cocrystal structure was solved by Synchrotron X-ray Diffraction and characterized using a combination of differential scanning calorimetry (DSC), X-ray powder diffraction (XRPD), infrared spectroscopy (FT-IR), solid-state NMR (SSNMR) and scanning electron microscopy (SEM). Physical and chemical stability under several conditions (i.e., drug recovery, physical stability as solid phase and in aqueous solution) were also investigated.

Finally, in vitro anthelminthic activity on Newly Transformed Schistosomula (NTS), and adult Schistosoma *mansoni* (S. *mansoni*) and in vivo preliminary tests on mice were carried out.

2. Materials and methods

2.1. Materials

PZQ (11bRS)-2-(Cyclohexylcarbonyl)-1,2,3,6,7,11b-hexahydro-4-H-pyrazino[2,1-a] isoquinolin-4-one] of Ph. Eur. grade was kindly donated by Fatro S.p.a. (Bologna, Italy), while NCM (5-chloro-N-(2-chloro-4-nitrophenyl)-2-hydroxybenzamide) was purchased from Sigma-Aldrich (St. Louis, USA) with a declared purity of 98–101 %. Methanol (MeOH) and ethyl acetate (EA) were provided from Carlo Erba (Rodano-Milan, Italy) and Normapur (Fontenay sous Bois, France), respectively. HPLC-grade hexane (HXN), ethanol (EtOH), isopropanol (IsOH), triethylene glycol (TEG), acetone (AcT), acetonitrile (ACN), 2-pyrrolidone (2-Pyr), dimethyl sulfoxide (DMSO) were purchased from Sigma-Aldrich (St. Louis, USA). All the actives and chemicals were used without further purification.

2.2. Methods

2.2.1. Preparation of the cocrystal

The mechanochemical synthesis of PZQ-NCM cocrystal was performed in Retsch MM400 vibrational mill (Retsch, Germany) equipped by two 25 mL stainless steel jars and one 10 mm Ø beads, respectively. After a set of preliminary trials where the drug-to-drug molar ratio, the amount and type of liquid and the milling time were varied, a phase pure cocrystal was obtained by milling 400 mg of PZQ-NCM mixture in a 1:3 molar ratio in the presence of 160 μL of methanol for 120 min at 25 Hz. The same outcome can be obtained milling 200 mg of powder by using two 15 mL stainless steel jars with two 7 mm Ø grinding balls in the presence of 80 μL of methanol for 120 min at 25 Hz. The new system was characterized by DSC, XRPD, SSNMR and FT-IR.

A single crystal of appropriate size for single-crystal X-ray diffraction (SXRD) analysis was obtained by conventional solution crystallization, starting from preformed seeds of PZQ-NCM cocrystal.

Specifically, 20 mg of the powdered cocrystal obtained through mechanochemistry was transferred in a 20 mL lidded vial and dissolved in 16 mL of ethyl acetate by stirring at room temperature. Subsequently, the lid was slightly pierced to let slow evaporation occur. Single crystals appeared after 15 days.

2.2.2. DSC analysis

For DSC analysis, each sample weighing 2–4 mg was introduced into an aluminum sealed and pierced 40 μL crucible and analyzed by a Mettler Toledo DSC 3 Star System (Milan, Italy) with a heating program of 30–240 °C (10 °C/min) under a nitrogen atmosphere (50 mL/min flow rate).

2.2.3. Laboratory XRPD analysis

Routine XRPD analysis was carried out by a Bruker D2 Phaser benchtop diffractometer (Bruker, Manheim, Germany) in the Bragg-Brentano geometry, using Cu-Kα radiation (λ = 1.5418 Å) with a 300 W low-power X-ray generator (30 kV at 10 mA). All the measurements were conducted in a 2θ range of 3–60° with a step size of 0.02° and a scan speed of 0.6°/s.

Each sample was prepared by gently pressing approximately 200 mg of ground product into the cavity of a steel sample holder equipped with a cylindrical polyvinylidene fluoride (PVDF) reducer.

2.2.4. FT-IR analysis

Powdered samples were analyzed with a Shimadzu IRAffinity-1S FT-IR instrument (Kyoto, Japan) in a range of 400–4000 cm^{-1} with a resolution of 4 cm^{-1} and 20 scans.

Suitable discs for analysis were prepared by gently grinding in an agate mortar 200 mg of anhydrous KBr (99 % infrared grade) with 1 % w/w of analyte and then pressing the mixture with a hydraulic press

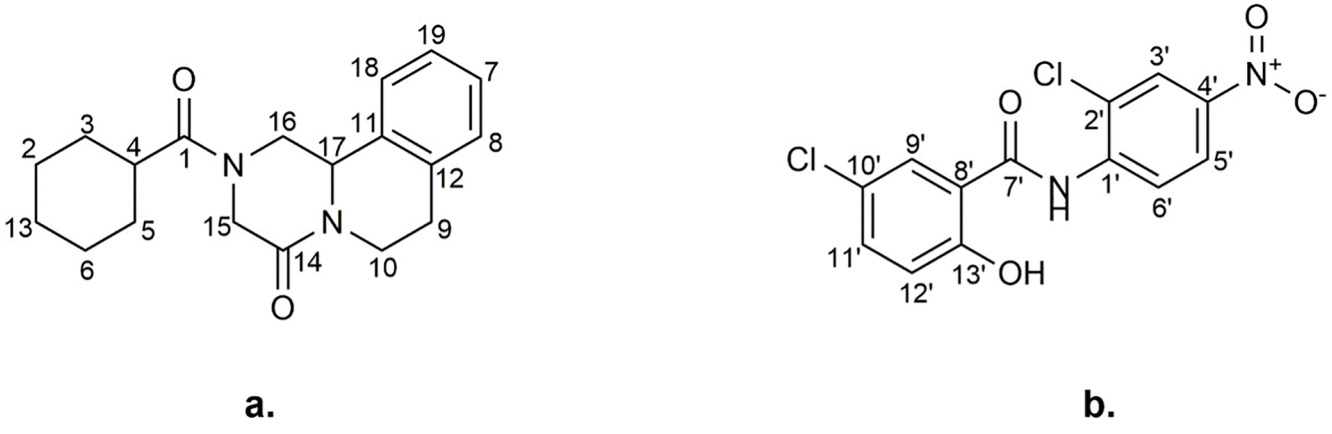

Fig. 1. (a) Praziquantel and (b) Niclosamide molecular structures with atom numbering.

(PerkinElmer, Norwalk, USA), applying a pressure of 10 Ton for 3 min.

2.2.5. SSNMR analysis

Solid-state NMR spectra were acquired with a Bruker Avance II 400 Ultra Shield instrument, operating at 400.23, 100.63 and 40.56 MHz, respectively for ^{1}H, ^{13}C and ^{15}N nuclei.

The powdered sample was packed into cylindrical zirconia rotors with a 4 mm o.d. and a, 80 μL volume. A certain amount of sample was collected from the batch and used without further preparations to fill the rotor. ^{13}C CPMAS spectra were acquired at a spinning speed of 12 kHz, using a ramp cross-polarization pulse sequence with a 90° ^{1}H pulse of 3.60 μs, a contact time of 3 ms, an optimized recycle delays of 17.3 s and a scans number of 4744. ^{15}N CPMAS spectra were acquired at a spinning speed of 9 kHz using a ramp cross-polarization pulse sequence with a 90° ^{1}H pulse of 3.60 μs, a contact time of 4 ms, an optimized recycle delays of 17.3 s and a scans number of 8700. For every spectrum, a two-pulse phase modulation (TPPM) decoupling scheme was used, with a radio-frequence field of 69.4 kHz. The ^{13}C and ^{15}N chemical shift scales were calibrated through the signals of γ-glycine (^{13}C methylenic peak at 43.7 ppm and ^{15}N peak at 33.4 ppm with reference to NH_3).

2.2.6. Synchrotron X-ray diffraction and solution of crystal structure

The data collection of the cocrystal obtained in powder form and single crystal were both performed the X-ray diffraction beamline (XRD2) of Elettra Synchrotron (Trieste, Italy) (Lausi et al., 2015).

Both the samples' data were acquired using monochromatic wavelength of 0.620 Å on Pilatusˆ M hybrid-pixel area detectors (DECTRIS Ltd., Baden-Daettwil, Switzerland). The powder sample was measured at 298 K in transmission mode filling a boron capillary of 0.5 mm of diameter. The single crystal was dipped in NHV oil (Jena Bioscience, Jena, Germany) and mounted on the goniometer head with kapton loops (MiTeGen, Ithaca, USA). Complete datasets were collected at 100 K and 298 K with a nitrogen stream supplied through an Oxford Cryostream 700, through the rotating crystal method. The diffraction data were indexed, integrated and scaled using XDS (Kabsch, 2010).The structures were solved by the dual space algorithm implemented in the SHELXT (Sheldrick, 2015a). Fourier analysis and refinement were performed by the full-matrix least-squares methods based on F^2 implemented in SHELXL (Version 2018/3) (Sheldrick, 2015b). The Coot program was used for modeling (Emsley et al., 2010). Geometry and thermal motion parameters restrain (SAME, DFIX, DANG and SIMU) have been used on disordered PZQ molecules. Hydrogen atoms were included at calculated positions with isotropic $U_{factors} = 1.2 \bullet U_{eq}$ or $U_{factors} = 1.5 \bullet U_{eq}$ for methyl and hydroxyl groups (U_{eq} being the equivalent isotropic thermal factor of the bonded non hydrogen atom). Pictures were prepared using Ortep-3 (Farrugia, 2012), CCDC Mercury (MacRae et al., 2020) and Pymol software (Schrodinger, 2015). Table 1 reports crystal data collection and refinement results. Related files can be obtained free of charge from The Cambridge Crystallographic Data Centre via https://www.ccdc.cam.ac.uk/structures.

2.2.7. SEM analysis

Images of PZQ-NCM cocrystal were collected through SEM. The powdered sample was placed on aluminum stubs covered with a carbon double-sided tape and sputter-coated with gold using a Sputter Coater K550X (Emitech, Quorum Technologies Ltd, UK), before being analyzed by a scanning electron microscope (Quanta 250 SEM, FEI, Oregon, USA) with the secondary electron detector. The working distance was set at 10 mm to obtain the appropriate magnifications, and the acceleration voltage was set at 30 kV.

2.2.8. Drug recovery

To check possible degradation of PZQ after milling, ^{1}H NMR spectra were recorded on a Bruker Avance 600 spectrometer equipped with a 14T superconducting magnet and two 5 mm probes. Analyzed samples (two different batches of the same cocrystal) were dissolved in deuterated dimethyl sulfoxide (DMSO-d_6) using tetramethyl silane (TMS) as reference. Measurements were performed at 300 K using a simple pulse-acquire sequence.

Table 1
Crystallographic data and refinement details for PZQ-NCM cocrystal at 298 K and 100 K.

	1PZQ3NCM	1PZQ3NCM
CCDC Number	2257493	2257492
Chemical Formula	C58H48Cl6N8O14	C58H48Cl6N8O14
Formula weight	1293.74 g/mol	1293.74 g/mol
Temperature	298(2) K	100(2) K
Wavelength	0.620 Å	0.620 Å
Crystal system	Monoclinic	Monoclinic
Space Group	*P* 21/*c*	*P* 21/*c*
Unit cell dimensions	$a = 13.465(3)$ Å	$a = 13.391(3)$ Å
	$b = 10.588(2)$ Å	$b = 10.389(2)$ Å
	$c = 40.090(8)$ Å	$c = 39.841(8)$ Å
	$\alpha = 90°$	$\alpha = 90°$
	$\beta = 97.62(3)°$	$\beta = 97.59(3)°$
	$\gamma = 90°$	$\gamma = 90°$
Volume	5665(2) Å^3	5494.1(19) Å^3
Z	4	4
Density (calculated)	1.517 g·cm^{-3}	1.564 g·cm^{-3}
Absorption coefficient	0.259 mm^{-1}	0.259 mm^{-1}
F(0 0 0)	2664	2664
Theta range for data collection	1.3°–31.1°	1.3°–31.1°
Index ranges	$-22 \le h \le 22$	$-22 \le h \le 22$
	$-17 \le k \le 17$	$-17 \le k \le 17$
	$-61 \le l \le 61$	$-61 \le l \le 61$
Reflections collected	134,317	129,076
Independent reflections (data with I > 2σ(I))	24,562 (19,327)	23,754 (22,858)
Resolution	0.60 Å	0.60 Å
Data multiplicity (max resltn)	4.82 (2.93)	4.77 (2.86)
I/σ(I) (max resltn)	31.42 (6.15)	50.40 (26.84)
Rmerge (max resltn)	0.0234 (0.1569)	0.0207 (0.0374)
Data completeness (max resltn)	89.7 % (73.2 %)	89.5 % (73.1 %)
Refinement method	Full-matrix least-squares on F^2	Full-matrix least-squares on F^2
Data/restraints/parameters	24,562/43/799	23,754/43/799
Goodness-of-fit on F^2	1.033	1.020
Δ/σmax	0.001	0.001
Final R indices [I > 2σ(I)]	$R_1 = 0.0499$	$R_1 = 0.0415$
	$wR_2 = 0.1457$	$wR_2 = 0.1041$
R indices (all data)	$R_1 = 0.0605$	$R_1 = 0.0432$
	$wR_2 = 0.1542$	$wR_2 = 0.1048$
Largest diff. peak and hole	0.371 and −0.459 eÅ^{-3}	0.602 and −0.500 eÅ^{-3}
R.M.S. deviation from mean	0.048 eÅ^{-3}	0.070 eÅ^{-3}

2.2.9. Cocrystal physical stability under several conditions

The solid-state stability of the PZQ-NCM was analyzed at room temperature (20 °C) by storing samples over a period of 12 months in a desiccator containing calcium chloride. At the end of such period, the stored samples were analyzed using XRPD, applying the operating conditions reported in Section 2.2.3.

The stability of the cocrystal in aqueous solution was also investigated to determine if homo- and heteromolecular hydrogen bonds are involved in improving the stability domain of PZQ-NCM cocrystal in comparison to the corresponding physical mixture in solution. About 250 mg of compressed powder were immersed together with a sample holder, previously used for intrinsic dissolution studies (Zanolla et al., 2018a), in a vessel containing 900 mL of a solution of distilled water with 0.5 % p/v of sodium lauryl sulfate, kept at 37 °C and stirred at 100 rpm. After 60 min, as the tablet was still intact and did not disintegrate, sample surface areas exposed to the medium was retrieved and analyzed through XRPD to detect any solid-state conversion. For comparison purposes, the corresponding physical mixture and pure APIs were subjected to the same procedure.

2.2.10. In vitro anthelmintic activity

In vitro and in vivo experiments were conducted in accordance with the local cantonal veterinary guidelines, license number 520. The in vitro anthelmintic activity of PZQ-NCM cocrystal was tested using Newly Transformed Schistosomula (NTS), which are immature Schistosoma, and adult *Schistosoma mansoni* (*S. mansoni*).

NTS and adult *S. mansoni* were obtained by transforming cercariae from infected *B. glabrata* snails. Adult *S. mansoni* of both sexes were collected from the hepatic portal system and mesenteric veins of infected mice.

NTS (n = 50) and *S. mansoni* (three pairs) were placed in the presence of culture media (M199 and RPMI culture medium supplemented with 1 % penicillin (10,000 U/mL) and streptomycin (10 mg/mL solution) in 96 and 24 well plates, respectively and kept at 37 °C for 72 h. Each plate contained concentrations of the samples, ranging from 0.1 to 1 μM. An additional concentration of 0.01 μM was also carried out for adult *S. mansoni* model.

The results were determined as the effect in percentage of worm activity reduction by microscopically observing the motility or damage to the tegument and changes to the morphology of NTS and adult *S. mansoni*. IC_{50} values were calculated using the CompuSyn software (ComboSyn Inc., Paramus, NJ., USA).

2.2.11. In vivo studies and ethics

Animals were ordered from Charles-River (Sulzfeld, Germany). A total of 12 three-week-old NMRI mice were used for this study. Upon arrival, the animals were left for one week for acclimatization. The animals were housed at 25 °C in a controlled environment (temperature ~ 25 °C; humidity ~ 70 %; 12-hour light and 12-hour dark cycle) with free access to water and rodent diet. The mice were infected subcutaneously with 100 *S. mansoni* cercaria in the neck area.

Seven weeks post-infection, mice (N = 4/group) were treated with 600 mg/kg (corresponding to about 150 mg of PZQ/kg and 450 mg of NCM/kg) of the cocrystal or physical mixture, as a powder.

For the oral administration, 6 hard gelatin capsules, size M (Torpac Europe BV, Heerlen, The Netherlands), were filled with the appropriate amount of powder and administered to each mouse. In this context, capsules provide a suitable method for the oral dosage to laboratory mice weighing about 33 g by using a Torpac® dosing syringe. This procedure eliminates validation of suspension/solution homogeneity and vehicle excipients absorption affects. The procedure, which can be performed rapidly by trained personnel, is ideally suited for dispensing solid materials to fully conscious animals.

After treatment, the mice were monitored daily, for the next 21 days, before undergoing CO_2 euthanasia. The mice were then dissected, and their livers were excised. Adult worms were picked, sexed, and counted as described in Section 2.2.10. The worm burden reduction (WBR) was calculated by comparing the average number of recovered worms from each treatment arm to the control arm. The detailed in vivo procedure is previously described by Lombardo et al. (2019a).

3. Results and discussion

3.1. Preparation of the cocrystal

The mechanochemical preparation of PZQ-NCM cocrystal was performed varying the drug-to-drug molar ratio, the amount and type of liquid and the time of grinding, one at a time. On the contrary, frequency was always maintained at 25 Hz, and the filling volume of jars was fixed in a ratio of 400 mg of sample in 25 mL of jar capacity.

Starting from the drug-to-drug molar ratio, the cocrystal synthesis was first attempted by creating various physical mixtures with different molar ratios of PZQ and NCM, whose DSC curves indicated best stoichiometries for generating the pure cocrystal (see Fig. S1 in the Supplementary Information (SI) file). Subsequently, mixtures of PZQ-NCM with 1:1, 1:2, 1:3 molar ratios were ground in LAG conditions and then analyzed by XRPD. PZQ-NCM 1:3 molar ratio provided the best outcome compared to the other molar ratios, since XRPD graphs confirmed the formation of a new solid phase without any unreacted residues of the two starting materials (see Fig. S2 in the SI file).

Given 120 min as the best grinding time, the type of liquid was also investigated.

The solvents were selected by considering liquids previously used for obtaining cocrystals of PZQ (e.g., EtOH, AcT, ACN, EA) (Cugovčan et al., 2017; Devogelaer et al., 2021; Espinosa-Lara et al., 2013; Liu et al., 2021; Yang et al., 2022)and NCM (e.g., IsOH, ACN) (Grifasi et al., 2015; Sanphui et al., 2012). Hexane, a commonly used liquid in LAG procedures (Wang et al., 2022) was also selected. All grinding liquids allowed for the cocrystallization of PZQ and NCM.

As a proof of concept, solvents able to form solvates with PZQ and NCM (e.g., 2-pyr, MeOH, TEG, DMSO, DMF) (de Villiers et al., 2004; MacEachern et al., 2021; Zanolla et al., 2021), initially excluded to avoid the formation of solvated forms as byproducts, were then used as grinding liquids. Surprisingly, also this set of liquids favored the formation of PZQ-NCM cocrystal with the exception for DMSO and 2-pyr without the insurgence of solvated forms. Methanol and hexane, having peculiarly different chemical properties, were the best catalytic liquids, as evident from XRPD results. Methanol resulted the preferred liquid for obtaining the new solid system with higher yield and crystallinity.

Table S1 lists all the liquid analyzed for the preparation of PZQ-NCM cocrystal, while Fig. S3 in the SI file reports the XRPD patterns of the ground solids.

The empirical parameter η (μL/mg) was maintained at LAG settings ($0 < \eta < 2$) to ensure catalytic conditions of the liquid (Friščić et al., 2009): precisely 160 μL of methanol were added to 400 mg of sample and the grinding process was carried out for 120 min at 25 Hz.

To summarize, a PZQ-NCM cocrystal was discovered by mechanochemical activation, presenting a very peculiar 1:3 stoichiometry that is somewhat unusual in the variety of cocrystals reported in literature.

3.2. DSC analysis

The thermal behavior of PZQ-NCM cocrystal was investigated by DSC, and results are reported in Fig. 2. Specifically, the thermogram of the cocrystal only showed an endothermic peak at 202.89 °C, with an enthalpy of 107.14 J/g, which was attributed to its melting point. The lack of additional endotherms testified the anhydrous nature of the solid and the absence of residual grinding liquid. This newly observed endothermic event clearly differs from the experimental melting points of raw PZQ and NCM, detected at 141.99 °C and 229.98 °C, respectively, both in agreement with literature data(Sanphui et al., 2012; Zanolla et al., 2018a).

3.3. XRPD analysis

The laboratory diffraction patterns of PZQ, NCM, PZQ-NCM cocrystal and the calculated pattern from PZQ-NCM single crystal are shown in Fig. 3. The diffraction pattern of the mechanochemically prepared cocrystal shows reflections at 4.53, 7.54, 13.32, 14.62, 16.39, 18.26, 22.52, 24.61, 26.11, 26.63, clearly different from their corresponding starting materials, and the absence of signals attributable to original coformers confirms the purity of the new solid phase.

3.4. FT-IR spectroscopy

FT-IR measurements were carried out on PZQ, NCM, PZQ-NCM cocrystal and the corresponding physical mixture. Fig. 4 shows only fragments of particular interest of the four spectra (see Fig. S4 in SI file for full spectra). Physical mixture is nothing but the sum of the signals of the pure APIs.

Differently from the physical mixture, N—H stretching and bending

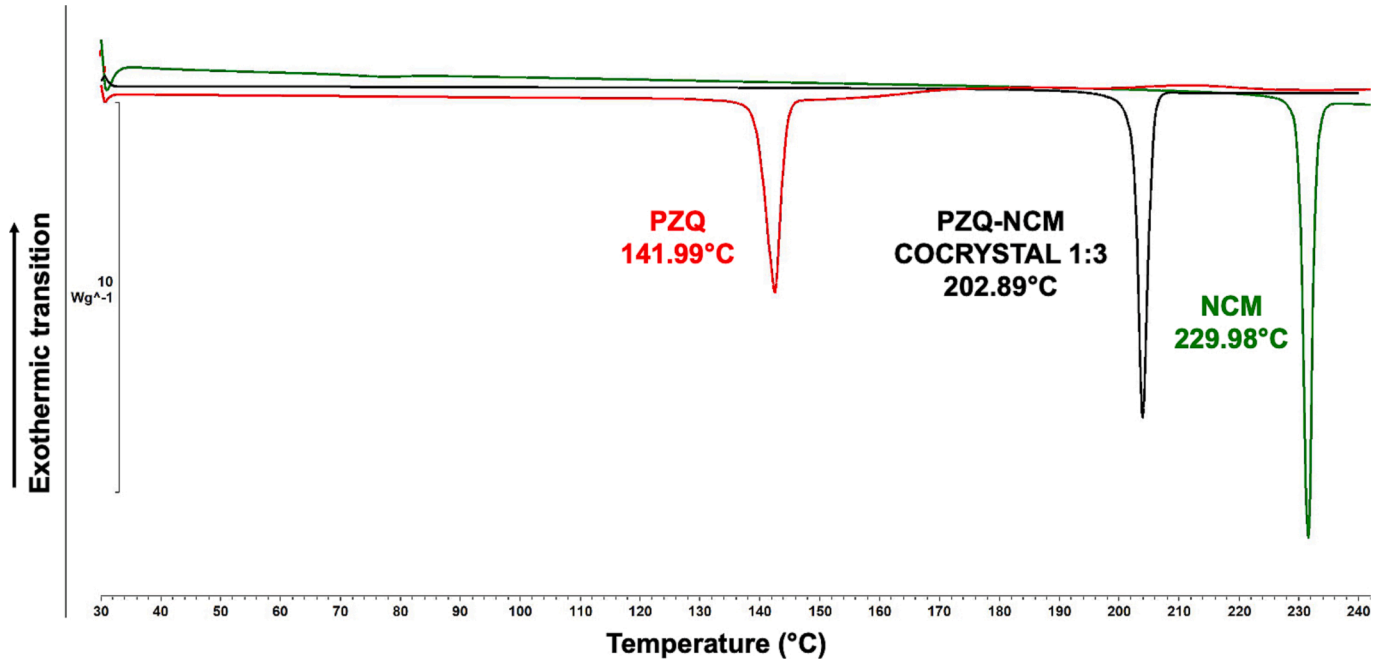

Fig. 2. DSC experimental curves of mechanochemically prepared PZQ-NCM cocrystal (black), raw PZQ (red) and raw NCM (green). (For interpretation of the references to colour in this figure legend, the reader is referred to the web version of this article.)

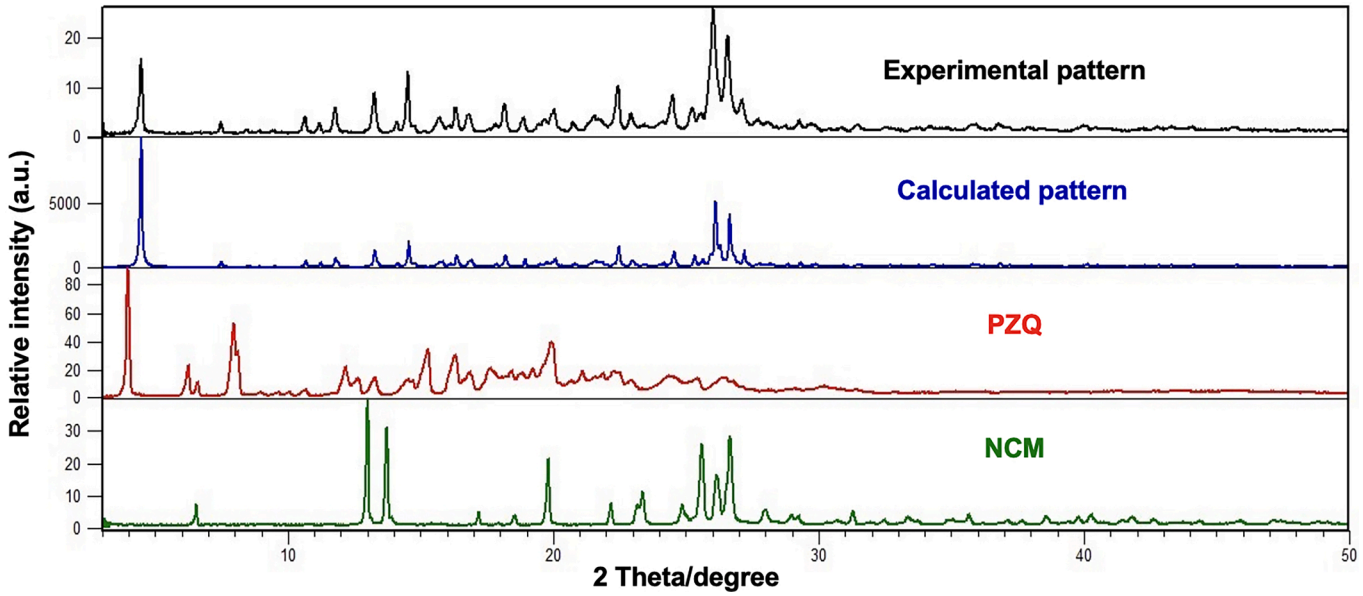

Fig. 3. XRPD of PZQ (red), NCM (green), and PZQ-NCM cocrystal obtained mechanochemically (black) and the calculated pattern from the single crystal (blue). (For interpretation of the references to colour in this figure legend, the reader is referred to the web version of this article.)

peaks of NCM, originally at 3241–3101 cm^{-1} and 897 cm^{-1}, respectively, in agreement with Bhushan et al., 2015, are downward shifted, suggesting involvement of NCM N—H group in H-bonds with PZQ. Moving to the typical range of C═O stretching, signals of PZQ carbonyl groups are markedly shifted in the cocrystal, forming a doublet at 1694 and 1684 cm^{-1}, while in the physical mixture the signal remains at 1650 cm^{-1} as in PZQ (Perissutti et al., 2017; Zanolla et al., 2018a), confirming intermolecular interactions between the two APIs. Moreover, signals of C—OH stretching of NCM can be seen at 1231 cm^{-1}, shifted at higher intensities in comparison to the raw NCM peak at 1219 cm^{-1} (Xie and Yao, 2018).

Therefore, it is worth to assume that the two C═O of PZQ and both N—H and C—OH signals of NCM are involved in molecular interactions between the two drugs in the cocrystal.

3.5. SSNMR analysis

The ^{13}C CPMAS spectrum recorded for the new system is shown in Fig. 5a, where it is compared with those of pure PZQ and NCM. The ^{13}C SSNMR spectrum of PZQ-NCM cocrystal presented no traces of unreacted starting materials. Besides comparing the spectrum with the starting materials (PZQ and NCM), it was also investigated if there was a conversion of PZQ in the polymorphic form B during the synthesis since form B is obtained by neat grinding form A for 4 h. However, it is evident

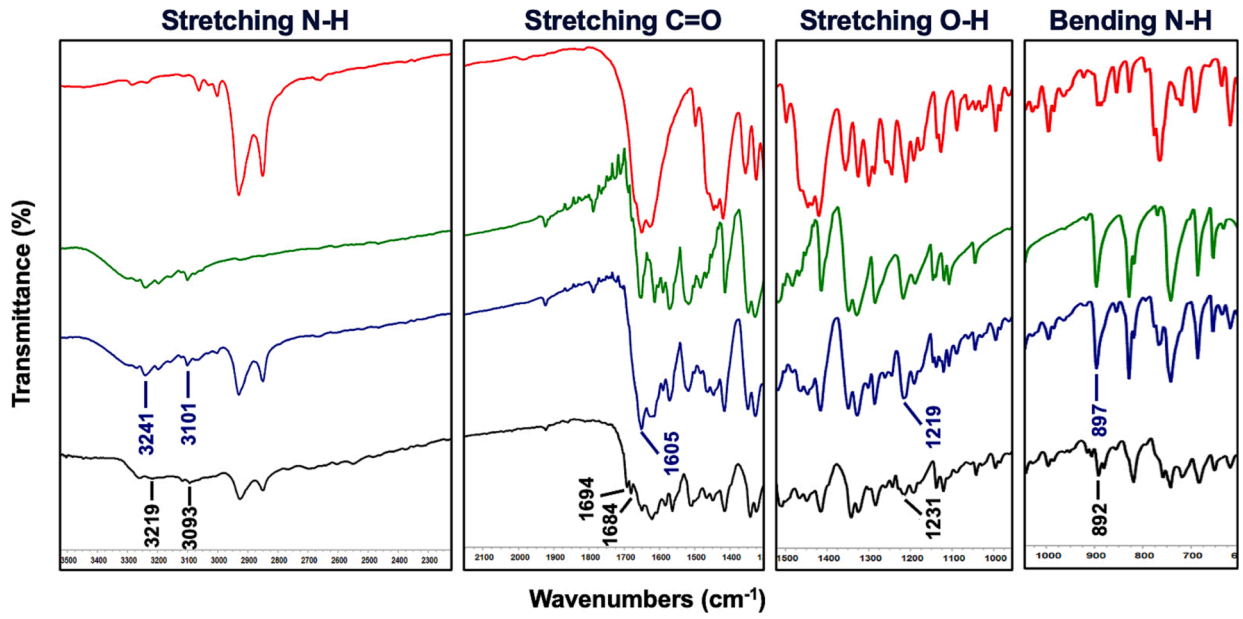

Fig. 4. FT-IR spectra of PZQ (red), NCM (green), PZQ-NCM physical mixture (blue) and PZQ-NCM cocrystal (black). (For interpretation of the references to colour in this figure legend, the reader is referred to the web version of this article.)

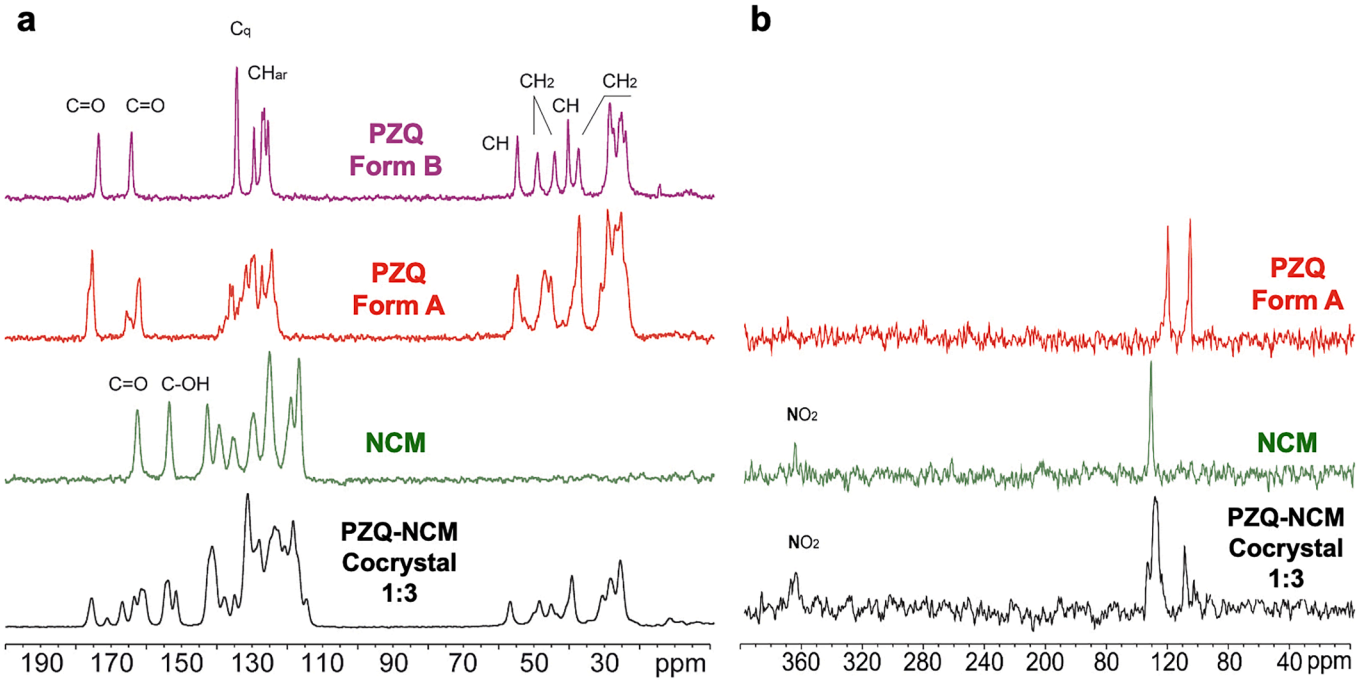

Fig. 5. (a) ^{13}C (100 MHz) CPMAS spectra with relevant assignments of PZQ-NCM cocrystal (black), pure NCM (green), pure PZQ (red) and PZQ form B (purple) acquired at a spinning speed of 12 kHz at room temperature. (b) ^{15}N (40.6 MHz) CPMAS spectra with relevant assignments of PZQ-NCM cocrystal (black), pure NCM (green) and pure PZQ (red), acquired at a spinning speed of 9 kHz at room temperature. (For interpretation of the references to colour in this figure legend, the reader is referred to the web version of this article.)

that the signals of the synthetized sample are not superimposable with those of the PZQ form B (purple spectrum in Fig. 5a) and the new signals are not due to a different polymorph of the starting material. So, the presence of new signals pattern leads to the conclusion that a new crystal form was obtained. The signals in the system exhibit an average full width half maximum value of ~160 Hz; this indicates a moderate degree of crystallinity. The aliphatic region of the sample shows significant changes in terms of both the shape of the signals and their chemical shifts, compared to the same region of the pure PZQ. The peaks between 25 and 35 ppm correspond to six CH_2 groups of PZQ (indicated in Fig. 1 as C5, C6, C13, C2, C3 and C9). Moving to higher frequencies, the second group of signals (35–55 ppm) is attributable to C16, C10 and C4 carbons of PZQ. Finally, the signals at 57.6 ppm are related to C17 and it shows a shift of 1.3 ppm compared to the pure PZQ (56.3 ppm).

The aromatic region (120–140 ppm) is difficult to assign and shows overlapping signals from the aromatic carbons of PZQ and NCM. The splitted signal at about 153 ppm is attributable to NCM C13′, while the signal at 175.6 is related to PZQ C1. These two signals, isolated in the

spectrum, were used to evaluate the stoichiometric ratio of the cocrystal: the number of signals agrees with the presence of one molecule of PZQ and three molecules of NCM *per* asymmetric unit.

Fig. 5b displays an analogous comparison between the ^{15}N CPMAS spectra of PZQ-NCM cocrystal and pure PZQ and NCM. The presence of a new signal pattern in the cocrystal ^{15}N spectrum confirms the formation of a new multicomponent system. The N amide and nitro group chemical shifts demonstrate the formation of supramolecular interactions between PZQ and NCM and a new crystalline packing. In addition, the split of the signals related to NCM confirms the stoichiometry PZQ-NCM 1:3.

3.6. Cocrystal structure solution

Fig. 6 shows PZQ-NCM single cocrystal obtained through crystallization by slow evaporation used for the crystal structure solution.

The XRPD pattern simulated from the single crystal used for the resolution of the cocrystal structure was in good agreement with the experimentally acquired XRPD pattern of the cocrystal (see Fig. 3).

The single crystal shows one PZQ and three NCM crystallographic independent molecules in the asymmetric unit (ASU) at 298 K. Data collected at 100 K confirm the same crystal form found at room temperature, with small cell volume contractions (~3 %). No solvent has been found inside the crystal packing, confirming the DSC results. All NCM molecules adopt a rigid, extended and planar conformation, defined by central amidic bond planarity constrain and homomolecular hydrogen bonds (with average dNH•••O = 2.65(1) Å and dNH•••Cl = 2.92(2) Å). NCM moieties bear extensive electronic delocalization and are prone to stack through π•••π interactions (average dπ•••π = 3.70(1) Å with 1.5 Å slippage between ring centroids). NCM molecules are coordinated to PZQ through hydrogen bonds (Table 2): the two PZQ carbonyl groups act as acceptors bound to NCM donor hydroxyl groups. The additional NCM present in the cocrystal ASU is linked to the carbonyl of one NCM bound to PZQ, confirming FT-IR results. The relative orientation of PZQ respect to NCM molecules is almost perpendicular in the cocrystal structure (Fig. 7). Interestingly, both PZQ carbonyl groups are oriented in a *syn* conformation, as in PZQ Form A (Zanolla et al., 2018a). This is an unusual feature, as all the PZQ cocrystals, reported in great number in literature, except for two (PZQ-malonic acid and PZQ- myricetin), exhibit an anti-conformation (Charpentier et al., 2022; Devogelaer et al., 2021; Espinosa-Lara et al., 2013; Liu et al., 2021; Yang et al., 2021, 2022).

The crystal structure results in a monoclinic unit cell with a space group of $P2_1/c$.

Centrosymmetric crystal packing is consistent with the usage of racemic PZQ which is also partially disordered in the ASUs, suggesting that the inversion of PZQ chirality does not alter its steric hindrance and conserve carbonyl acceptors positions (i.e., without altering the hydrogen bond network that keeps molecules tightly bound).

3.7. SEM analysis

Fig. 8 shows SEM images of PZQ, NCM and PZQ-NCM powdered cocrystal. The newly cocrystal form consisted of agglomerates of small plates (more evident at higher magnifications), showing a habitus clearly different from the reported needle-shaped particles of PZQ (Perissutti et al., 2017) and the peculiar rectangles with protrusions of NCM (Van Tonder et al., 2004). The particle size of the plates varies in the range 150–1500 nm, as roughly determined by Fiji/Imagej software (Schindelin et al., 2012).

3.8. Drug recovery

From literature is well-known the degradation tendency of PZQ under milling conditions (Perissutti et al., 2017; Šagud et al., 2018; Zanolla et al., 2018b). While PZQ did not degrade upon milling when the drug was milled alone (Zanolla et al., 2019, 2018a), in binary ground mixes a diminished drug recovery was noticed with the insurgence of peculiar degradation products as a function of the excipient used (Perissutti et al., 2017; Šagud et al., 2018; Zanolla et al., 2018b).Therefore, spectrometric evaluations have been carried out to understand whether PZQ undergoes chemical degradation when ground in the presence of NCM upon LAG conditions.

Recorded ^1H NMR spectra in DMSO-d_6 showed only the presence of the starting materials PZQ and/or NCM, attesting the lack of chemical changes both in PZQ and NCM after mechanochemical treatment under all experimental conditions. The absence of any new signal in the two different batches analyzed indicates that there are no new structures present in the samples. Based on all obtained information and comparison of the crucial parts of the ^1H NMR spectra of PZQ (a), NCM (b), cocrystal batch n°1 (c) and cocrystal batch n°2 (d) (see Fig. S5 in SI file),

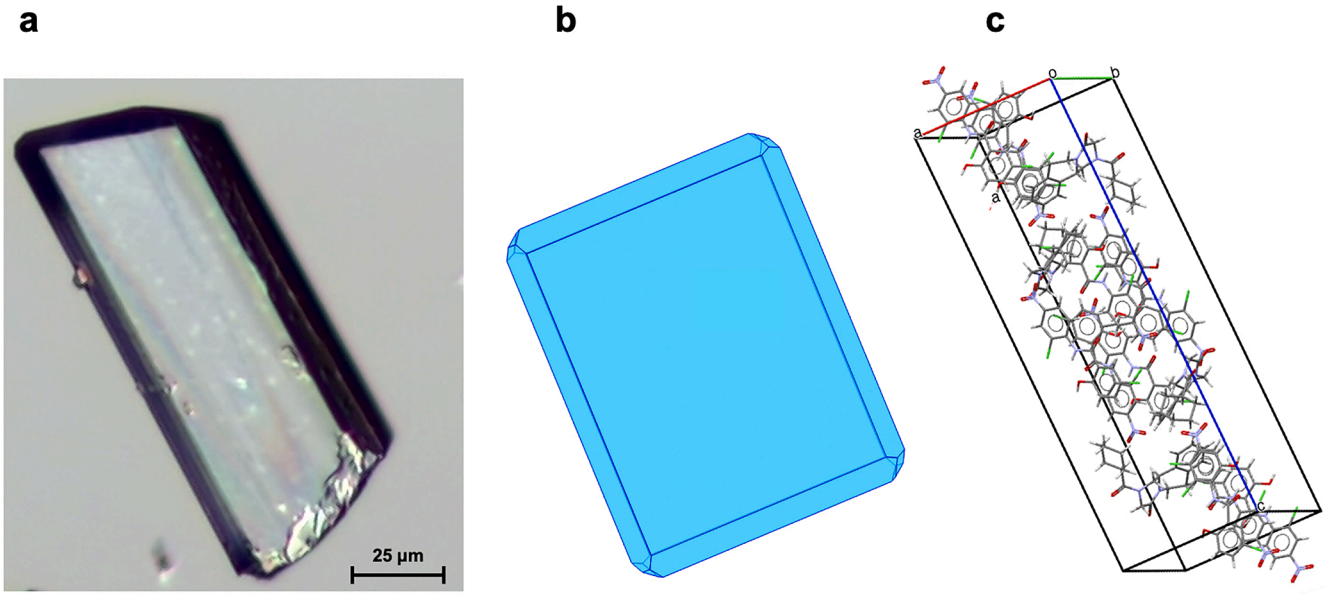

Fig. 6. (a) Optical image of PZQ-NCM single crystal obtained through solution crystallization at a magnification of 10×, (b) BFDH morphology, (c) orientation of PZQ and NCM molecules into the unit cell.

Table 2
Geometrical parameters of hydrogen bonds found in PZQ-NCM cocrystal at 298 K and 100 K.

1PZQ3NCM at 298 K				
D-H···A	d(D-H) (Å)	d(H···A) (Å)	d(D···A) (Å)	<(DHA) (°)
O4_2-H4_2×××O1_1	0.82	1.82	2.642(2)	177.0
O4_3-H4_3×××O2_1	0.82	1.80	2.617(2)	175.0
O4_4-H4_4×××O3_3	0.82	1.92	2.721(2)	164.8
N2_2-H2_2×××Cl1_2	0.86	2.44	2.923(1)	116.3
N2_3-H2_3×××Cl1_3	0.86	2.40	2.891(1)	116.4
N2_4-H2_4×××Cl1_4	0.86	2.46	2.941(1)	115.7
N2_2-H2_2×××O4_2	0.86	1.93	2.653(2)	141.0
N2_3-H2_3×××O4_3	0.86	1.92	2.636(2)	140.2
N2_4-H2_4×××O4_4	0.86	1.93	2.653(2)	141.4

1PZQ3NCM at 100 K				
D-H···A	**d(D-H) (Å)**	**d(H···A) (Å)**	**d(D···A) (Å)**	**<(DHA) (°)**
O4_2-H4_2×××O1_1	0.84	1.80	2.635(1)	177.9
O4_3-H4_3×××O2_1	0.84	1.77	2.607(1)	174.3
O4_4-H4_4×××O3_3	0.84	1.88	2.695(1)	164.2
N2_2-H2_2×××Cl1_2	0.88	2.43	2.927(1)	115.8
N2_3-H2_3×××Cl1_3	0.88	2.39	2.887(1)	116.4
N2_4-H2_4×××Cl1_4	0.88	2.45	2.940(1)	115.3
N2_3-H2_3×××O4_3	0.88	1.90	2.637(1)	140.2
N2_2-H2_2×××O4_2	0.88	1.91	2.653(1)	140.9
N2_4-H2_4×××O4_4	0.88	1.91	2.651(2)	141.3

a high chemical stability of PZQ and NCM under the applied grinding conditions is confirmed.

3.9. Physical stability under several conditions

PZQ-NCM cocrystal was periodically analyzed by XRPD for 12 months to check for possible modifications. Indeed, there are examples in the literature where the presence of defects on the surface of crystalline solids (Eddleston et al., 2022) or different humidity conditions (Thakuria et al., 2019) are reported as possible precursors/factors for cocrystal dissociation. Further, since anhydrous NCM is known to transform to greenish monohydrate H_A within one month of storage at ambient conditions (Sanphui et al., 2012), the aim of checking PZQ-NCM cocrystal stability was also to recognize the insurgence of the hydrate. The hydrate formation is highly undesired as it exhibits a solubility even lower than anhydrous NCM. The physical stability results, reported in Fig. S6 in the SI file, attested that the new multicomponent system remained unchanged over a period of 12 months, with no signs of cocrystal dissociation of hydrate formation.

Further, in the context of PZQ-NCM cocrystal physical stability in aqueous solution, a flat tablet of PZQ-NCM cocrystal was immersed in an aqueous solution for 60 min. After that time, the solid sample was retrieved and analyzed through XRPD and DSC to visualize any solid-state conversion. The same procedure was adopted for corresponding PZQ-NCM physical mixture, pure PZQ and NCM.

XRPD and DSC results are displayed in Fig. 9. No phase conversion was visualized for raw PZQ after 60 min of exposure to medium. Conversely, pure NCM and PZQ-NCM physical mixture showed a rapid transformation into the well-known monohydrate H_A (Sanphui et al., 2012; Van Tonder et al., 2004). Instead, PZQ-NCM cocrystal maintained its crystalline integrity in aqueous solution, preventing thus the formation of poorly soluble NCM monohydrate H_A. In accordance with previous studies (Port et al., 2019; Sanphui et al., 2012), this cocrystal is an example of a solid with a very stable profile and distinctive properties in aqueous solutions, ameliorated with respect to pure coformers and their free combination.

This means that PZQ-NCM cocrystal structure provides several peculiar features versus the simple PZQ-NCM physical mixture and the conformers alone in relation to its physical stability in aqueous solution. The differential behavior of the cocrystal over the physical mixture is attributable to the PZQ-NCM supramolecular interactions imparting strength to the cocrystal lattice (NCM molecules are linked together and with PZQ molecules through hydrogen bonds in the 3D supramolecular network, as previously mentioned). In literature one can find other examples of cocrystal with similar aqueous stability, such as those reported by (Port et al., 2019; Sanphui et al., 2012). In relation to the individual components, and in particular to NCM, thanks to the supramolecular

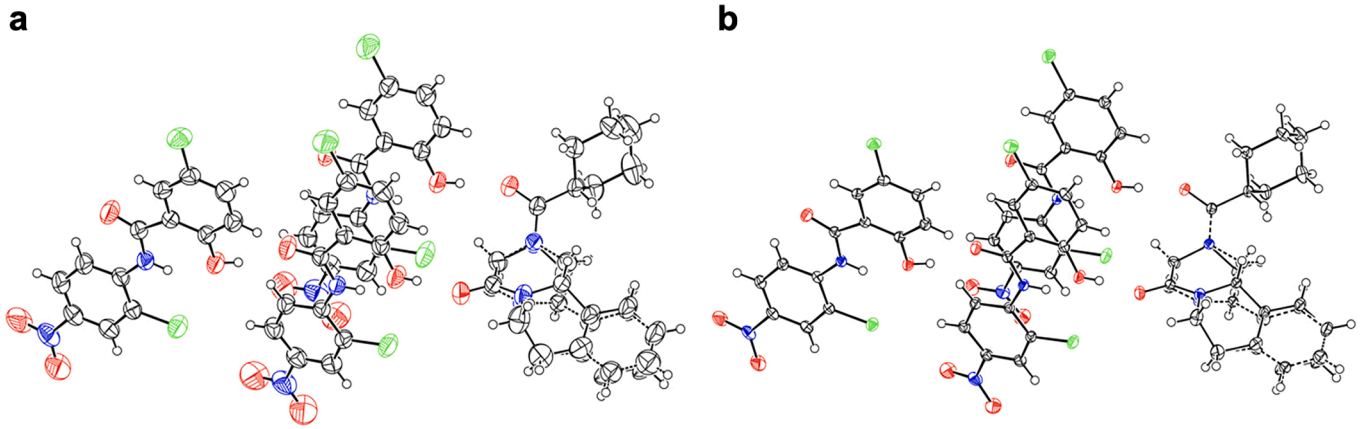

Fig. 7. Ellipsoids representation of ASU contents (50 % probability) for PZQ-NCM cocrystal at 298 K (a) and 100 K (b).

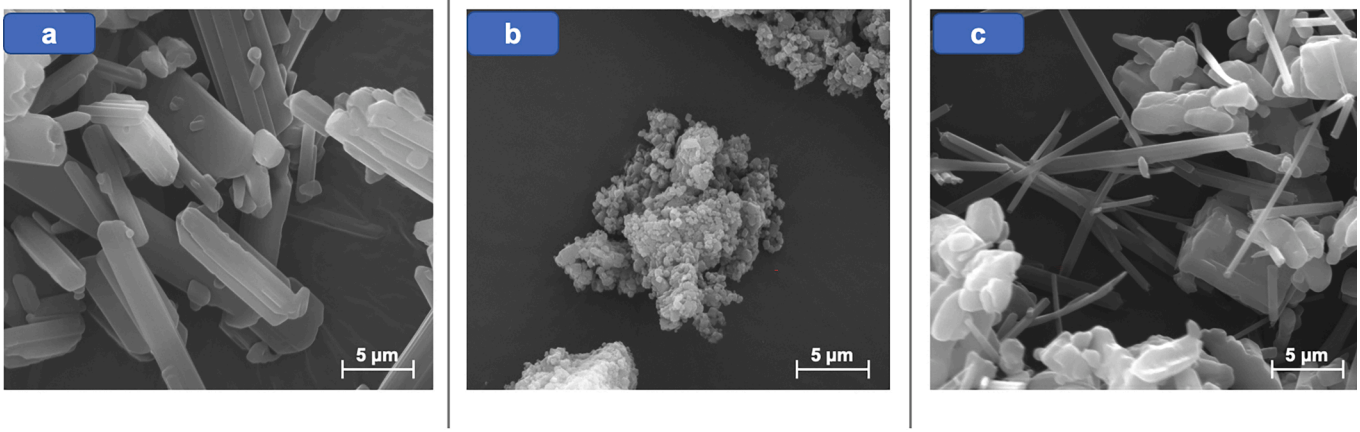

Fig. 8. SEM images of (a) PZQ, (b) PZQ-NCM cocrystal and (c) NCM at a magnification of 5000×.

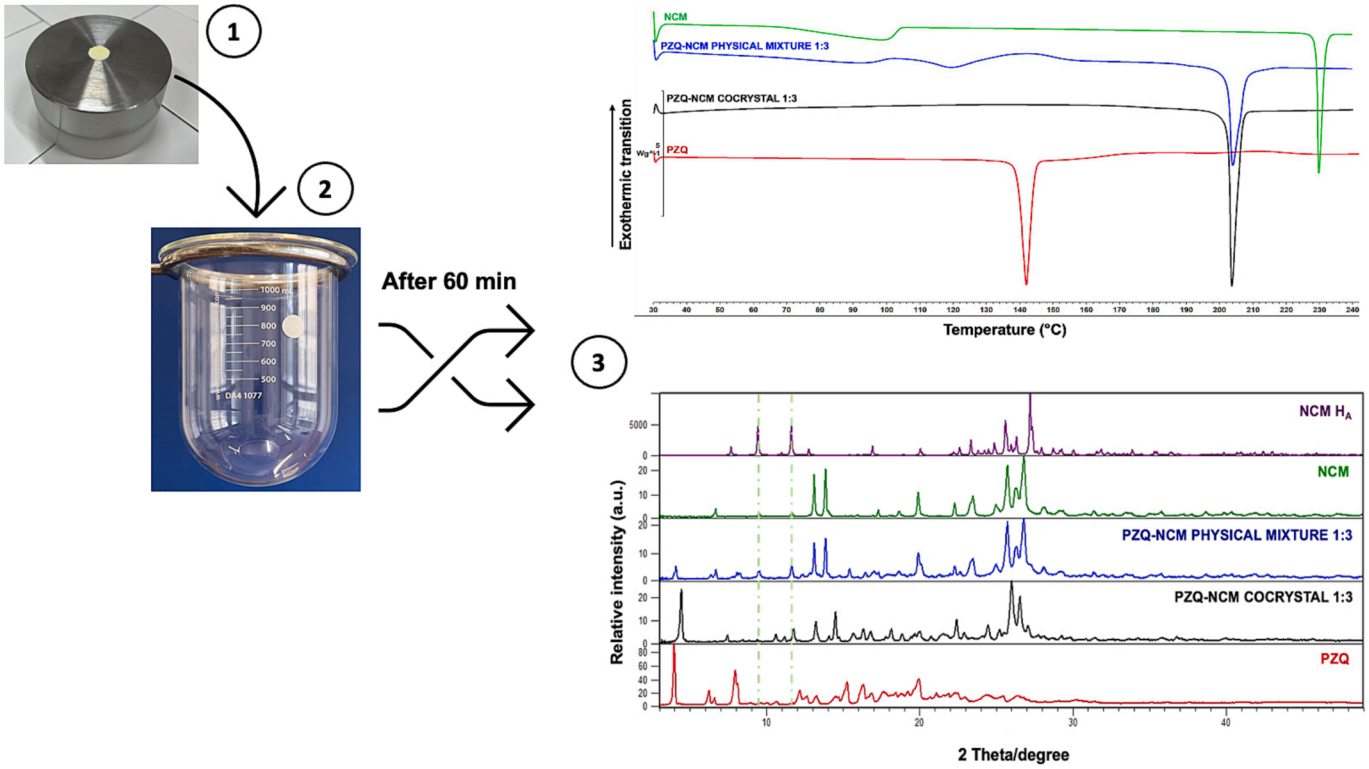

Fig. 9. Schematic representation of the investigation of cocrystal physical stability in aqueous solution: (1) compressed powder in the intrinsic dissolution sample holder, (2) vessel containing the aqueous solution, (3) DSC and XRPD results of solid samples retrieved after 60 min of exposure to the medium.

Table 3
In vitro anthelmintic activity after 72 h on NTS and *S. mansoni* adults in vitro models of PZQ-NCM 1:3 cocrystal and corresponding physical mixture having the same composition.

Samples	NTS			*S. mansoni* adult			
	Effect in % (dead, 72 h) + SD		IC50 (µM)(72 h) Dm	Effect in % (dead, 72 h) +SD			IC50 (µM)(72 h) Dm
	Testconc. 1 µM	Testconc. 0.1 µM		Testconc. 1 µM one round	Testconc. 0.1 µM one round	Testconc. 0.01 µM one round	
Physical mixture 1:3	100 (0)	28.85 (1.9)	0.12282	100 (0)	53.9 (2)		0.09610
Cocrystal 1:3	92.31 (3.8)	25 (1.9)	0.20256	100 (0)	71.95 (4)	39.55 (6.3)	0.02123

interactions, the cocrystal structure confers a resistance to the otherwise predominant transition into the undesired monohydrate NCM H_A having even lower solubility than NCM (0.45–0.55 mg/L) and characterized by a cement-like behavior in aqueous suspension (Sanphui et al., 2012).

3.10. In vitro anthelmintic activity

In vitro NTS and *S. mansoni* models were placed in well plates with variable concentrations of two cocrystal batches and the corresponding PZQ-NCM physical mixture. Effects were rated microscopically by observing the motility or damage to the tegument and changes to the morphology of NTS and *S. mansoni* adults.

Results in Table 3 attests that, in the case of *S. mansoni* adults, the new 1:3 cocrystal exhibits higher efficacy than that observed for PZQ-NCM physical mixture at 0.1 μM. As for the NTS, results show that mechanochemical treatment and cocrystallization have no negative effects on in vitro activity. In fact, PZQ-NCM cocrystal has no significative difference in response compared to the physical mixture of the two API.

3.11. In vivo preliminary tests

In vivo pilot tests were performed on PZQ-NCM cocrystal and compared to pure PZQ and the corresponding physical mixture (Table 4). Interestingly, to mimic the administration praxis of the two API (marketed as solid oral tablets), the samples were administered as a powder in minicapsules size M (specific for mice), instead of the conventional aqueous suspensions, commonly used during in vivo administration in animal subjects (Lombardo et al., 2019b).

When compared to methods used in previous studies, such procedure prevents regurgitation and revulsion of the animal to the bitter taste of the drug and allows the administration of the correct dose. Additionally, this procedure avoids the use of excipients or solvents that may interfere with the API absorption or with animal physiology, allowing a proper comparison of different solid forms.

Even though these are preliminary results on a limited number of subjects coming from the difficulties of administering 6 capsules to each mouse, and though the high variability of the results, it can be attested that there was no significant difference between the number of worms recovered from infected mice treated with cocrystal or physical mixture.

Considering the treatment with pure PZQ capsules, a comparison with the cocrystal is ineffective due to un underdosage compared to PZQ monotherapy. Despite this limitation, it is worth mentioning that the administration of capsules filled with the pure component is somewhat a positive control group, since it confirms that the treatment with minicapsules worked. Therefore, higher doses of cocrystal administered in minicapsules result promising for future in vivo studies.

4. Conclusions

A novel drug-drug antiparasitic cocrystal consisting of praziquantel and niclosamide in a 1:3 molar ratio is proposed for the first time. The novel PZQ-NCM cocrystal, showing this very peculiar stoichiometry, relatively uncommon in cocrystallization field, can be obtained through a sustainable one-step mechanochemical process in the presence of micromolar amount of common solvents in 120 min. Even though the mechanochemical cocrystallization was found not to be particularly influenced by the type of solvent for LAG experiments, methanol was finally preferred as adjuvant liquid for its higher efficiency. The phase was obtained as pure solid, without traces of unreacted starting coformers and absence of residual solvent. The same 1:3 cocrystal can be obtained in 2 weeks by conventional solution crystallization, starting from preformed seeds of PZQ-NCM cocrystal.

The novel solid phase crystallized in the monoclinic space group of $P2_1/c$, showing one PZQ and three NCM molecules linked through homo- and heteromolecular hydrogen bonds in the ASU, confirming SSNMR and FT-IR results.

The new 1:3 cocrystal exhibited a plate-like habitus, as evident from SEM analysis, and a melting point of 202.89 °C, which was intermediate to those of PZQ and NCM.

No typical PZQ tendency of decay was seen in the experimental grinding conditions and the cocrystal showed a very stable profile under several conditions. In the context of physical stability in aqueous solution, the new multicomponent system provided a higher efficiency in avoiding solid-state transformation into NCM monohydrate, in comparison to PZQ-NCM physical mixture. Cocrystal solid-state remained unchanged over a period of 12 months at ambient temperature, with no signs of dissociation in the parent compounds or transition in NCM monohydrate, typically insurging within one month of storage at ambient conditions.

More importantly, in vitro anthelmintic activity was carried out: PZQ-NCM cocrystal exhibited higher anthelmintic activity (%-effect of activity reduction) against in vitro *S. mansoni* models than that observed for PZQ-NCM 1:3 physical mixture and, in the case of NTS, the new system showed no significative difference in response compared to APIs physical mixture.

Finally, considering in vitro promising results, in vivo preliminary tests were also performed on the cocrystal, pure PZQ and corresponding physical mixture: despite the limited number of mice treated, there was no significant difference between the number of worms recovered from infected mice treated with cocrystal or physical mixture. In the case of treatment with pure PZQ, a comparison with the cocrystal was ineffective due to an underdosage compared to PZQ monotherapy. Nevertheless, the administration of pure PZQ to mice resulted a positive control group, since it confirmed that the treatment with minicapsules worked, showing that higher doses of cocrystal are encouraging for future in vivo studies.

Table 4
Effect of cocrystal, physical mixture and raw PZQ (administered as oral minicapsules size M) on the worm burden reduction (WBR) in mice harboring a chronic *S. mansoni* infection.

Application date: 09. November 2022/Dissection date 30.11–01.12.2022		
Sample	Average of WBR %	Number of mice
PZQ around 300 mg/kg with capsules	91.11	4
PZQ-NCM physical mixture 1:3 around 600 mg/kg with capsules	15.56	2*
PZQ-NCM Cocrystal 1:3 around 600 mg/kg with capsules	4.44	4

*Treated 4 mice, but 2 died during treatment.

CRediT authorship contribution statement

Ilenia D'Abbrunzo: Visualization, Methodology, Validation, Formal analysis, Investigation, Resources, Software, Writing – original draft. **Emma Bianco:** Methodology, Validation, Formal analysis, Investigation, Resources, Writing – original draft. **Lara Gigli:** Visualization, Methodology, Validation, Formal analysis, Investigation, Resources, Software, Writing – original draft. **Nicola Demitri:** Visualization, Methodology, Validation, Formal analysis, Investigation, Resources, Software, Writing – original draft. **Rebecca Birolo:** Visualization, Methodology, Validation, Formal analysis, Investigation, Resources, Writing – original draft. **Michele R. Chierotti:** Writing – review & editing, Methodology, Validation, Formal analysis, Investigation, Resources. **Irena Škorić:** Writing – original draft, Methodology, Validation, Formal analysis, Investigation, Resources. **Jennifer Keiser:** Writing – review & editing, Writing – original draft, Methodology, Validation, Formal analysis, Investigation, Resources. **Cécile Häberli:** Methodology, Validation, Formal analysis, Investigation, Resources. **Dario Voinovich:** Funding acquisition, Methodology, Validation, Formal analysis, Investigation, Resources. **Dritan Hasa:** Supervision,

Writing – review & editing, Methodology, Validation, Formal analysis, Investigation, Resources. **Beatrice Perissutti:** Supervision, Writing – review & editing, Conceptualization, Methodology, Validation, Formal analysis, Investigation, Resources, Project administration, Funding acquisition.

Declaration of Competing Interest

The authors declare that they have no known competing financial interests or personal relationships that could have appeared to influence the work reported in this paper.

Data availability

The cocrystal structure has been deposited in the CCDC with these numbersCCDC number 2257492-3.

Acknowledgments

Authors wish to thank Davide Porrelli for assistance for SEM analysis and Paolo Pengo for cooperation in FT-IR analysis. We also acknowledge the NMR Centre at Ruđer Bošković Institute and the competent help by Željko Marinić for recording all the NMR spectra.

Appendix A. Supplementary material

Crystallographic information files (CIF) and Check CIF files for PZQ-NCM cocrystal at 298 K and 100 K, indexed in CCDC as 2257493 and 2257492, respectively. Related files can be obtained free of charge from The Cambridge Crystallographic Data Centre via https://www.ccdc.cam.ac.uk/structures.

Supplementary data to this article can be found online at https://doi.org/10.1016/j.ijpharm.2023.123315.

References

Bhushan, B., Dubey, P., Kumar, S.U., Sachdev, A., Matai, I., Gopinath, P., 2015. Bionanotherapeutics: Niclosamide encapsulated albumin nanoparticles as a novel drug delivery system for cancer therapy. RSC Adv. 5, 12078–12086. https://doi.org/10.1039/c4ra15233f.

Charpentier, M.D., Devogelaer, J.-J., Tijink, A., Meekes, H., Tinnemans, P., Vlieg, E., De Gelder, R., Johnston, K., Ter Horst, J.H., 2022. Comparing and quantifying the efficiency of cocrystal screening methods for praziquantel. Cryst. Growth Des. 22, 5525. https://doi.org/10.1021/acs.cgd.2c00615.

Cioli, D., Pica-Mattoccia, L., Basso, A., Guidi, A., 2014. Schistosomiasis control: praziquantel forever? Mol. Biochem. Parasitol. 195 (1), 23–29. https://doi.org/10.1016/j.molbiopara.2014.06.002.

Cugovčan, M., Jablan, J., Lovrić, J., Cinčić, D., Galić, N., Jug, M., 2017. Biopharmaceutical characterization of praziquantel cocrystals and cyclodextrin complexes prepared by grinding. J. Pharm. Biomed. Anal. 137, 42–53. https://doi.org/10.1016/j.jpba.2017.01.025.

de Villiers, M.M., Mahlatji, M.D., Malan, S.F., van Tonder, E.C., Liebenberg, W., 2004. Physical transformation of niclosamide solvates in pharmaceutical suspen-sions determined by DSC and TG analysis. Die Pharmazie 59 (7), 534–540. PMID: 15296091.

Deka, P., Gogoi, D., Althubeiti, K., Rao, D.R., Thakuria, R., 2021. Mechanosynthesis, characterization, and physicochemical property investigation of a favipiravir cocrystal with theophylline and GRAS coformers. Cryst. Growth Des. 21, 4417–4425. https://doi.org/10.1021/acs.cgd.1c00339.

Devogelaer, J.J., Charpentier, M.D., Tijink, A., Dupray, V., Coquerel, G., Johnston, K., Meekes, H., Tinnemans, P., Vlieg, E., Ter Horst, J.H., De Gelder, R., 2021. Cocrystals of praziquantel: discovery by network-based link prediction. Cryst. Growth Des. 21, 3428–3437. https://doi.org/10.1021/acs.cgd.1c00211.

Eddleston, M.D., Chow, E.H.H., Bučar, D.-K., Thakuria, R., 2022. Crystal surface defects as possible origins of cocrystal dissociation. CrstEngComm 24, 5031–5035. https://doi.org/10.1039/D2CE00166G.

Emsley, P., Lohkamp, B., Scott, W.G., Cowtan, K., 2010. Features and development of Coot. Acta Crystallogr. D Biol. Crystallogr. 66, 486–501. https://doi.org/10.1107/S0907444910007493.

Espinosa-Lara, J.C., Guzman-Villanueva, D., Arenas-García, J.I., Herrera-Ruiz, D., Rivera-Islas, J., Román-Bravo, P., Morales-Rojas, H., Höpfl, H., 2013. Cocrystals of active pharmaceutical ingredients - praziquantel in combination with oxalic, malonic, succinic, maleic, fumaric, glutaric, adipic, and pimelic acids. Cryst. Growth Des. 13, 169–185. https://doi.org/10.1021/cg301314w.

Farrugia, L.J., 2012. WinGX and ORTEP for Windows: an update. J. Appl. Cryst. 45, 849–854. https://doi.org/10.1107/S0021889812029111.

Friščić, T., Childs, S.L., Rizvi, S.A.A., Jones, W., 2009. The role of solvent in mechanochemical and sonochemical cocrystal formation: a solubility-based approach for predicting cocrystallisation outcome. CrstEngComm 11, 418–426. https://doi.org/10.1039/B815174A.

Grifasi, F., Chierotti, M.R., Gaglioti, K., Gobetto, R., Maini, L., Braga, D., Dichiarante, E., Curzi, M., 2015. Using salt cocrystals to improve the solubility of niclosamide. Cryst. Growth Des. 15, 1939–1948. https://doi.org/10.1021/acs.cgd.5b00106.

Kabsch, W., 2010. XDS. Acta Crystallogr. D Biol. Crystallogr. 66, 125–132. https://doi.org/10.1107/S0907444909047337.

Lausi, A., Polentarutti, M., Onesti, S., Plaisier, J.R., Busetto, E., Bais, G., Barba, L., Cassetta, A., Campi, G., Lamba, D., Pifferi, A., Mande, S.C., Sarma, D.D., Sharma, S. M., Paolucci, G., 2015. Status of the crystallography beamlines at Elettra. Eur. Phys. J. Plus 130 (3), 43. https://doi.org/10.1140/epjp/i2015-15043-3.

Lindenberg, M., Kopp, S., Dressman, J.B., 2004. Classification of orally administered drugs on the World Health Organization Model list of Essential Medicines according to the biopharmaceutics classification system. Eur. J. Pharm. Biopharm. 58 (2), 265–278. https://doi.org/10.1016/j.ejpb.2004.03.001.

Liu, Q., Yang, D., Chen, T., Zhang, B., Xing, C., Zhang, L., Lu, Y., Du, G., 2021. Insights into the solubility and structural features of four praziquantel cocrystals. Cryst. Growth Des. 21, 6321–6331. https://doi.org/10.1021/acs.cgd.1c00785.

Lombardo, F.C., Pasche, V., Panic, G., Endriss, Y., Keiser, J., 2019a. Life cycle maintenance and drug-sensitivity assays for early drug discovery in *Schistosoma mansoni*. Nat. Protoc. 14, 461–481. https://doi.org/10.1038/s41596-018-0101-y.

Lombardo, F.C., Perissutti, B., Keiser, J., 2019b. Activity and pharmacokinetics of a praziquantel crystalline polymorph in the *Schistosoma mansoni* mouse model. Eur. J. Pharm. Biopharm. 142, 240–246. https://doi.org/10.1016/j.ejpb.2019.06.029.

Luedeker, D., Gossmann, R., Langer, K., Brunklaus, G., 2016. Crystal engineering of pharmaceutical co-crystals: "nMR Crystallography" of niclosamide co-crystals. Cryst. Growth Des. 16, 3087–3100. https://doi.org/10.1021/acs.cgd.5b01619.

MacEachern, L.A., Walwyn-Venugopal, R., Kermanshahi-pour, A., Mirmehrabi, M., 2021. Ternary phase diagram development and production of niclosamide-urea co-crystal by spray drying. J. Pharm. Sci. 110, 2063–2073. https://doi.org/10.1016/j.xphs.2020.11.036.

MacRae, C.F., Sovago, I., Cottrell, S.J., Galek, P.T.A., McCabe, P., Pidcock, E., Platings, M., Shields, G.P., Stevens, J.S., Towler, M., Wood, P.A., 2020. Mercury 4.0: from visualization to analysis, design and prediction. J. Appl. Cryst. 53, 226–235. https://doi.org/10.1107/S1600576719014092.

Perissutti, B., Passerini, N., Trastullo, R., Keiser, J., Zanolla, D., Zingone, G., Voinovich, D., Albertini, B., 2017. An explorative analysis of process and formulation variables affecting comilling in a vibrational mill: the case of praziquantel. Int. J. Pharm. 533, 402–412. https://doi.org/10.1016/j.ijpharm.2017.05.053.

Port, A., Almansa, C., Enrech, R., Bordas, M., Plata-Salamán, C.R., 2019. Differential solution behavior of the new API-API co-crystal of tramadol-celecoxib (CTC) versus its constituents and their combination. Cryst. Growth Des. 19, 3172–3182. https://doi.org/10.1021/acs.cgd.9b00008.

Šagud, I., Zanolla, D., Perissutti, B., Passerini, N., Škorić, I., 2018. Identification of degradation products of praziquantel during the mechanochemical activation. J. Pharm. Biomed. Anal. 159, 291–295. https://doi.org/10.1016/j.jpba.2018.07.002.

Sanphui, P., Kumar, S.S., Nangia, A., 2012. Pharmaceutical cocrystals of niclosamide. Cryst. Growth Des. 12, 4588–4599. https://doi.org/10.1021/cg300784v.

Sarmah, K.K., Nath, N., Rao, D.R., Thakuria, R., 2020. Mechanochemical synthesis of drug–drug and drug–nutraceutical multicomponent solids of olanzapine. CrstEngComm 22, 1120–1130. https://doi.org/10.1039/C9CE01504C.

Schindelin, J., Arganda-Carreras, I., Frise, E., Kaynig, V., Longair, M., Pietzsch, T., Preibisch, S., Rueden, C., Saalfeld, S., Schmid, B., Tinevez, J.Y., White, D.J., Hartenstein, V., Eliceiri, K., Tomancak, P., Cardona, A., 2012. Fiji: An open-source platform for biological-image analysis. Nat. Methods 9 (7), 676–682. https://doi.org/10.1038/nmeth.2019.

Schrodinger, L., 2015. The PyMOL Molecular Graphics System [WWW Document]. URL http://www.pymol.org (accessed 4.4.23).

Sheldrick, G.M., 2015a. SHELXT - Integrated space-group and crystal-structure determination. Acta Crystallogr. A 71, 3–8. https://doi.org/10.1107/S2053273314026370.

Sheldrick, G.M., 2015b. Crystal structure refinement with SHELXL. Acta Crystallogr. C Struct. Chem. 71, 3–8. https://doi.org/10.1107/S2053229614024218.

Song, L., Robeyns, K., Tumanov, N., Wouters, J., Leyssens, T., 2020. Combining API in a dual-drug ternary cocrystal approach. Chem. Commun. 56, 13229–13232. https://doi.org/10.1039/d0cc05788f.

Thakuria, R., Delori, A., Jones, W., Lipert, M.P., Roy, L., Rodríguez-Hornedo, N., 2013. Pharmaceutical cocrystals and poorly soluble drugs. Int. J. Pharm. 453, 101–125. https://doi.org/10.1016/j.ijpharm.2012.10.043.

Thakuria, R., Arhangelskis, M., Eddleston, M.D., Chow, E.H.H., Sarmah, K.K., Aldous, B. J., Krzyzaniak, J.F., Jones, W., 2019. Cocrystal dissociation under controlled humidity: a case study of caffeine-glutaric acid cocrystal polymorphs. Org. Process Res. Dev. 23, 845–851. https://doi.org/10.1021/acs.oprd.8b00422.

Thakuria, R., Sarma, B., 2018. Drug-drug and drug-nutraceutical cocrystal/salt as alternative medicine for combination therapy: a crystal engineering approach. Crystals (Basel) 8, 101. https://doi.org/10.3390/cryst8020101.

Thipparaboina, R., Kumar, D., Chavan, R.B., Shastri, N.R., 2016. Multidrug co-crystals: towards the development of effective therapeutic hybrids. Drug Discov. Today 21, 481–490. https://doi.org/10.1016/j.drudis.2016.02.001.

Van Tonder, E.C., Maleka, T.S.P., Liebenberg, W., Song, M., Wurster, D.E., De Villiers, M. M., 2004. Preparation and physicochemical properties of niclosamide anhydrate and two monohydrates. Int. J. Pharm. 269, 417–432. https://doi.org/10.1016/j.ijpharm.2003.09.035.

Wang, X., Du, S., Zhang, R., Jia, X., Yang, T., Zhang, X., 2021. Drug-drug cocrystals: opportunities and challenges. Asian J. Pharm. Sci. 16, 307–317. https://doi.org/10.1016/j.ajps.2020.06.004.

Wang, L., Li, S., Xu, X., Xu, X., Wang, Q., Li, D., Zhang, H., 2022. Drug-drug cocrystals of theophylline with quercetin. J. Drug Deliv. Sci. Technol. 70, 103228 https://doi.org/10.1016/J.JDDST.2022.103228.

Xie, Y., Yao, Y., 2018. Octenylsuccinate hydroxypropyl phytoglycogen enhances the solubility and in-vitro antitumor efficacy of niclosamide. Int. J. Pharm. 535, 157–163. https://doi.org/10.1016/j.ijpharm.2017.11.004.

Yang, D., Cao, J., Heng, T., Xing, C., Yang, S., Zhang, L., Lu, Y., Du, G., 2021. Theoretical calculation and structural analysis of the cocrystals of three flavonols with praziquantel. Cryst. Growth Des. 21, 2292–2300. https://doi.org/10.1021/acs.cgd.0c01706.

Yang, S., Liu, Q., Ji, W., An, Q., Song, J., Xing, C., Yang, D., Zhang, L., Lu, Y., Du, G., 2022. Cocrystals of praziquantel with phenolic acids: discovery, characterization, and evaluation. Molecules 27, 2022. https://doi.org/10.3390/molecules27062022.

Zanolla, D., Perissutti, B., Passerini, N., Chierotti, M.R., Hasa, D., Voinovich, D., Gigli, L., Demitri, N., Geremia, S., Keiser, J., Cerreia Vioglio, P., Albertini, B., 2018a. A new soluble and bioactive polymorph of praziquantel. Eur. J. Pharm. Biopharm. 127, 19–28. https://doi.org/10.1016/j.ejpb.2018.01.018.

Zanolla, D., Perissutti, B., Passerini, N., Invernizzi, S., Voinovich, D., Bertoni, S., Melegari, C., Millotti, G., Albertini, B., 2018b. Milling and comilling Praziquantel at cryogenic and room temperatures: assessment of the process-induced effects on drug properties. J. Pharm. Biomed. Anal. 153, 82–89. https://doi.org/10.1016/j.jpba.2018.02.018.

Zanolla, D., Perissutti, B., Vioglio, P.C., Chierotti, M.R., Gigli, L., Demitri, N., Passerini, N., Albertini, B., Franceschinis, E., Keiser, J., Voinovich, D., 2019. Exploring mechanochemical parameters using a DoE approach: crystal structure solution from synchrotron XRPD and characterization of a new praziquantel polymorph. Eur. J. Pharm. Sci. 140, 105084 https://doi.org/10.1016/j.ejps.2019.105084.

Zanolla, D., Gigli, L., Hasa, D., Chierotti, M.R., Arhangelskis, M., Demitri, N., Jones, W., Voinovich, D., Perissutti, B., 2021. Article mechanochemical synthesis and physicochemical characterization of previously unreported praziquantel solvates with 2-pyrrolidone and acetic acid. Pharmaceutics 13 (10), 1606. https://doi.org/10.3390/pharmaceutics13101606.

Žegarac, M., Lekšić, E., Šket, P., Plavec, J., Devčić Bogdanović, M., Bučar, D.-K., Dumić, M., Meštrović, E., 2014. A sildenafil cocrystal based on acetylsalicylic acid exhibits an enhanced intrinsic dissolution rate. CrstEngComm 16, 32–35. https://doi.org/10.1039/C3CE42013B.

Supporting information

Praziquantel meets Niclosamide: A dual-drug Antiparasitic Cocrystal

Ilenia D'Abbrunzo[a], Emma Bianco[a], Lara Gigli[b], Nicola Demitri[b], Rebecca Birolo[c], Michele R. Chierotti[c], Irena Škorić[d], Jennifer Keiser[e,f], Cécile Häberli[e,f], Dario Voinovich[a], Dritan Hasa[a,]*, Beatrice Perissutti[a,]*

[a]*Department of Chemical and Pharmaceutical Sciences, University of Trieste, P.le Europa 1, 34127 Trieste, Italy; ILENIA.D'ABBRUNZO@phd.units.it*

[b]*Elettra-Sincrotrone Trieste, S.S. 14 Km 163.5 in Area Science Park, Basovizza–Trieste, Italy; lara.gigli@elettra.eu (L.G.); nicola.demitri@elettra.eu (N.D.)*

[c]*Department of Chemistry and NIS Centre, University of Torino, V. Giuria 7, 10125 Torino, Italy; michele.chierotti@unito.it*

[d]*Department of Organic Chemistry, Faculty of Chemical Engineering and Technology, University of Zagreb, Marulićev trg 19, 10000 Zagreb, Croatia*

[e]*Department of Medical Parasitology, Swiss Tropical and Public Health Institute, 4123 Allschwil, Switzerland.*
[f]*University of Basel, Basel 4000 Switzerland*

Contents

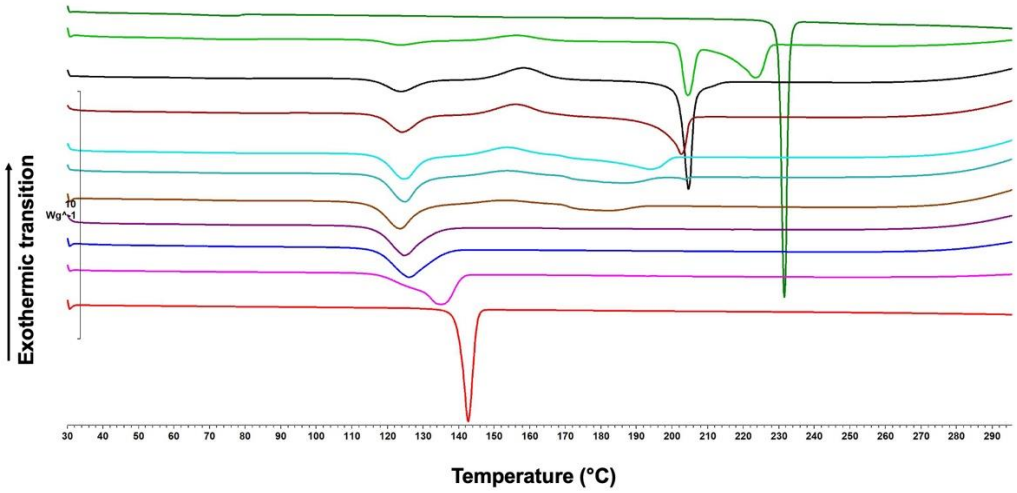

Figure S1. DSC curves of pure PZQ (red), pure NCM (dark green) and various physical mixtures with different molar ratios of PZQ and NCM: PZQ-NCM 0.10-0.90 (light green), PZQ-NCM 0.25-75 (black), PZQ-NCM 0.33-0.67 (dark red), PZQ-NCM 0.44-0.56 (light blue), PZQ-NCM 0.50-0.50 (aquamarine), PZQ-NCM 0.56-0.44 (brown), PZQ-NCM 0.67-0.33 (violet), PZQ-NCM 0.75-0.25 (blue), PZQ-NCM 0.90-0.10 (pink).

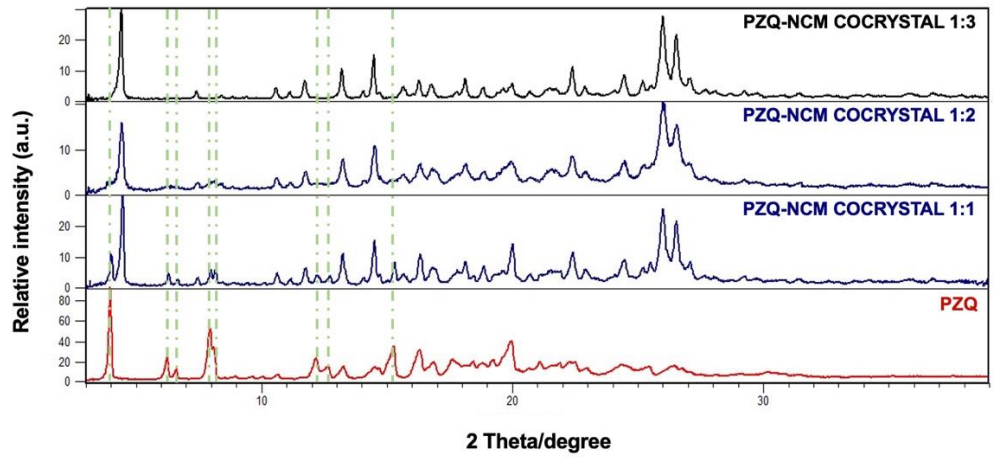

Figure S2. XRPD comparison of PZQ-NCM coground in different molar ratios.

Table S1. Different liquids investigated for LAG according to their polarity, protic properties and previously reported for PZQ and NCM cocrystals and solvates formation.

	Not previously used for cocrystals or solvates	Previously used for PZQ cocrystals or solvates	Previously used for NCM cocrystals or solvates
Non-polar	HXN		
Polar and protic		• EtOH	• IsOH • MeOH • TEG
Polar and aprotic		• EA • AcT:ACN 1:1 • 2-Pyr	• DMSO • DMF*

*Not used for toxicity reasons.

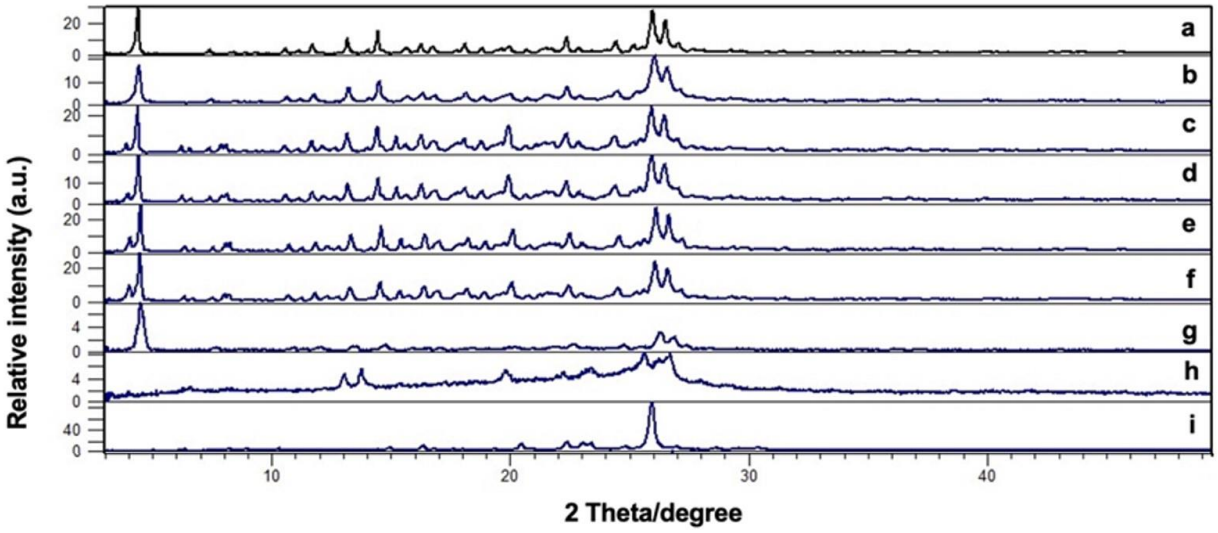

Figure S3. XRPD comparison of PZQ-NCM coground in 1:3 molar ratio in the presence of MeOH (a), HXN (b), TEG (c), EA (d), AcT-ACN (e), EtOH (f), IsOH (g), DMSO (h), 2-Pyr (i).

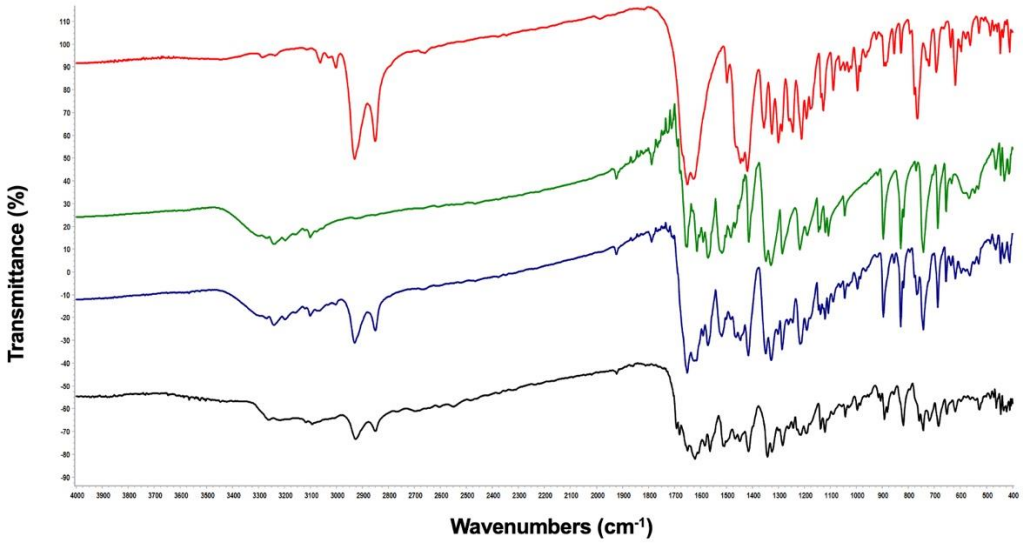

Figure S4. FT-IR full spectra of PZQ (red), NCM (green), PZQ-NCM physical mixture (blue) and PZQ-NCM cocrystal (black).

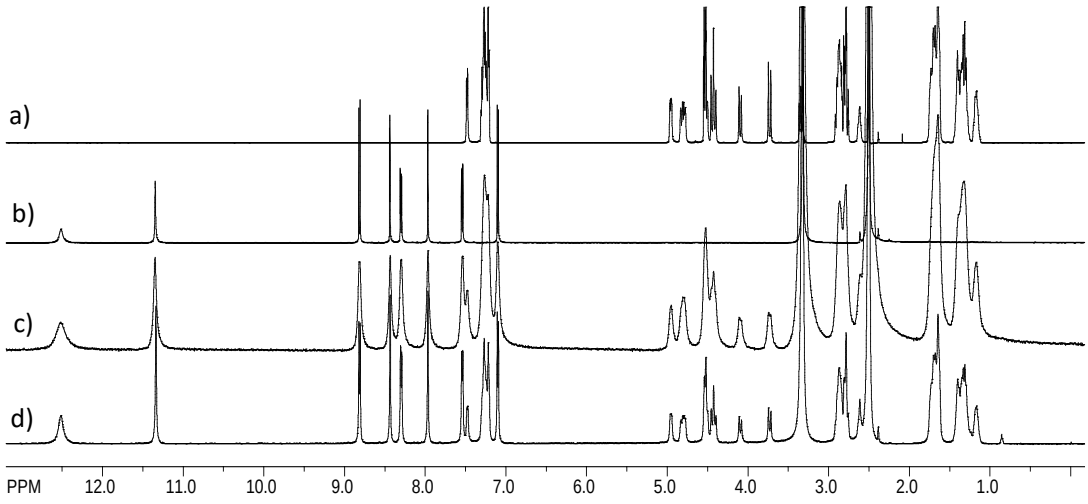

Figure S5. Comparison of the ^{1}H NMR spectra (DMSO-d_6) of PZQ (a), NCM (b), cocrystal batch n°1 (c) and batch n°2 (d).

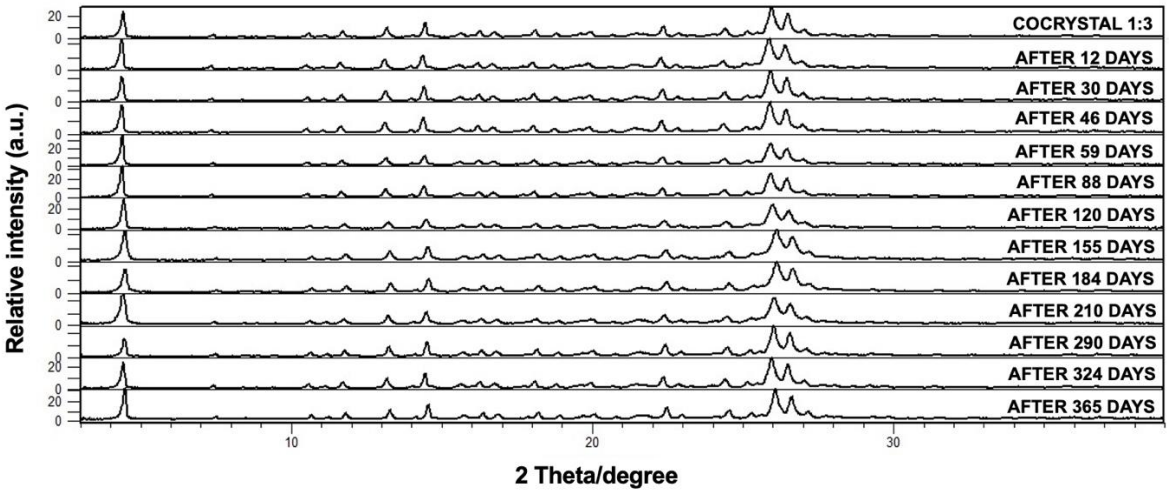

Figure S6. XRPD comparison of PZQ-NCM cocrystal over time.